Dobslaw, H., Bergmann-Wolf, I., Forootan, E., Dahle, C., Mayer-Gürr, T., Kusche, J., Flechtner, F. (2016): Modeling of present-day atmosphere and ocean non-tidal de-aliasing errors for future gravity mission simulations. - *Journal of Geodesy*, *90*, 5, pp. 423—436.

DOI: http://doi.org/10.1007/s00190-015-0884-3

Journal of Geodesy manuscript No.
(will be inserted by the editor)

Modeling of Present-Day Atmosphere and Ocean Non-Tidal De-Aliasing Errors for Future Gravity Mission Simulations

Henryk Dobslaw · Inga Bergmann-Wolf · Ehsan Forootan · Christoph Dahle · Torsten Mayer-Gürr · Jürgen Kusche · Frank Flechtner

Received: date / Accepted: date

Abstract A realistically perturbed synthetic de-aliasing model consistent with the updated Earth System Model of the European Space Agency is now available over the period 1995 – 2006. The data-set contains realizations of (i) errors at large spatial scales assessed individually for periods between 10 – 30, 3 – 10, and 1 – 3

H. Dobslaw
Deutsches GeoForschungsZentrum GFZ, Department 1: Geodesy and Remote Sensing, Telegrafenberg, 14473 Potsdam, Germany. Tel.: +49-331-288 1974, E-mail: dobslaw@gfz-potsdam.de

I. Bergmann-Wolf
Deutsches GeoForschungsZentrum GFZ Department 1: Geodesy and Remote Sensing, Telegrafenberg, 14473 Potsdam, Germany. Tel.: +49-331-288 1770 E-mail: ingab@gfz-potsdam.de

E. Forootan
Bonn University, Institute of Geodesy and Geoinformation, Nussallee 17, 53115 Bonn, Germany. Tel.: +49-228-73-6423, E-mail: forootan@geod.uni-bonn.de

Ch. Dahle
Deutsches GeoForschungsZentrum GFZ, Department 1: Geodesy and Remote Sensing, c/o DLR Oberpfaffenhofen, 82234 Wessling, Germany. Tel.: +49-8153-28-1589, E-mail: dahle@gfz-potsdam.de

T. Mayer-Gürr
Graz University of Technology, Institute for Geodesy, Steyrergasse 30/III, 8010 Graz, Austria. Tel.: +43-316-873-6359, E-mail: mayer-guerr@tugraz.at

J. Kusche
Bonn University, Institute of Geodesy and Geoinformation, Nussallee 17, 53115 Bonn, Germany. Tel.: +49-228-73-2629, E-mail: jkusche@geod.uni-bonn.de

F. Flechtner
Deutsches GeoForschungsZentrum GFZ, Department 1: Geodesy and Remote Sensing, c/o DLR Oberpfaffenhofen, 82234 Wessling, Germany. Tel.: +49-8153-28-1297, E-mail: flechtne@gfz-potsdam.de

days, the S1 atmospheric tide, and sub-diurnal periods; (ii) errors at small spatial scales typically not covered by global models of atmosphere and ocean variability; and (iii) errors due to physical processes not represented in currently available de-aliasing products. The model is provided in two separate sets of Stokes coefficients to allow for a flexible re-scaling of the overall error level to account for potential future improvements in atmosphere and ocean mass variability models. Error magnitudes for the different frequency bands are derived from a small ensemble of four atmospheric and oceanic models. For the largest spatial scales up to d/o = 40 and periods longer than 24 h, those error estimates are approximately confirmed from a variance component estimation based on GRACE daily normal equations. Future mission performance simulations based on the updated Earth System Model and the realistically perturbed de-aliasing model indicate that for GRACE-type missions only moderate reductions of de-aliasing errors can be expected from a second satellite pair in a shifted polar orbit. Substantially more accurate global gravity fields are obtained when a second pair of satellites in an moderately inclined orbit is added, which largely stabilizes the global gravity field solutions due to its rotated sampling sensitivity.

Keywords Time-Variable Gravity Field · Future Missions · Atmosphere and Ocean De-Aliasing Errors

1 Introduction

Observations from the twin-satellite mission GRACE (*Tapley et al.*, 2004) allow one to solve for a unique global gravity field model from observations accumulated over a time period of typically 30 days. After 13 years of operation, GRACE-based time-series representing month-to-month changes in the external gravitational field of the Earth offer the opportunity to infer variations of the water masses in the soil and sub-surface acquifers (*Famiglietti and Rodell*, 2013), and the continental ice-sheets (*Sasgen et al.*, 2013) down to spatial scales of a few 100 km. Such changes in the amount of water stored on the continents are characterized by rather low frequencies that are well resolved by a monthly sampling. In contrast to this, mass redistributions in the atmosphere, as, e.g., associated with the advection of cyclones, or in the oceans in response to time-variable surface winds, are dominated by much shorter periods. Since those mass signals are of similar or even greater magnitude than terrestrial water storage changes, their effects need to be properly treated in the gravity field estimation process to avoid temporal aliasing of high-frequency variability into the monthly mean gravity fields (*Thompson*, 2004; *Han et al.*, 2004).

The Atmosphere and Ocean De-Aliasing Product (AOD1B; *Flechtner and Dobslaw*, 2013) is routinely calculated by the GRACE Science Data System to provide a time-variable background model for the removal of non-tidal high-frequency mass signals from the sensor data. The most recent release 05 of AOD1B is based on 6 hourly sampled global atmospheric analysis fields from the European Centre for Medium Range Weather Forecasts (ECMWF) and an unconstrained simulation with the global ocean circulation model OMCT (*Dobslaw et al.*, 2013). In addition to this widely applied standard model, alternative atmosphere and ocean de-aliasing (AOD) coefficients are calculated by, e. g., Groupe de Recherche de

Geodesie Spatiale (GRGS; *Boy*, 2005), TU Munich (*Zenner et al.*, 2010), and University of Bonn (*Forootan et al.*, 2013). Imperfections in any of those de-aliasing models, however, will lead directly to residual atmospheric and oceanic signals in the instrument data that inevitably alias into the monthly mean gravity field solution. Such artifacts are frequently assumed to be one of the major reasons that the GRACE baseline accuracy targeted prior to the launch of the mission (*Kim*, 2000) is still not reached by the most recent data releases (*Sakumura et al.*, 2014).

While the GRACE Follow-On mission is progressing well towards its anticipated launch date in August 2017 (*Flechtner et al.*, 2014), mission performance simulation studies are carried out already now by several research groups in order to eventually propose concepts for future gravity missions to the space agencies (e.g., *Panet et al.*, 2012; *Gruber et al.*, 2014). Such simulations evaluate costs and benefits of higher sensor accuracies, orbits at lower altitudes that even might require active drag compensation, or constellations of multiple satellites connected by inter-satellite ranging links. In those studies, de-aliasing errors are typically either approximated from the difference of two arbitrarily selected numerical models (*Wiese et al.*, 2009, 2012; *Loomis et al.*, 2011) or by assuming that the errors are linearly dependent on the signal magnitude (*Visser*, 2010; *Elsaka et al.*, 2014). Both approaches lead to widely different magnitudes of de-aliasing errors, and consequently widely different conclusions about limiting factors on the overall accuracy of a future mission candidate concept.

We therefore attempt in this study to consolidate the present-day level of non-tidal atmosphere and ocean de-aliasing errors and prepare a realization of such errors that is readily applicable in future mission simulation studies together with the updated Earth System Model (ESM; *Dobslaw et al.*, 2015) of the European Space Agency (ESA). In the following, we discuss a strategy to approximate errors at large spatial scales that are typically well represented by global numerical atmosphere and ocean models (Sect. 2); and at small spatial scales that are only resolved by high-resolution regional models (Sect. 3). We further assess effects of physical processes that are not covered by a typical AOD model (Sect. 4), and describe how all those errors are made publicly available as part of the updated ESM (Sect. 5). Subsequently, a variance component estimation with present-day daily GRACE normal equations is performed to demonstrate the consistency of our error estimates with observational evidence (Sect. 6), and full-scale simulation experiments for both a GRACE setting and two double-pair configurations are carried out in order to assess the impact of those atmosphere and ocean non-tidal background model errors on the performance of future gravity missions (Sect. 7), before a brief summary is provided in Sect. 8.

2 AOD Errors at Large Spatial Scales

The mass variability in atmosphere and ocean represented by any AOD model currently available is inevitably contaminated by errors of the underlying geophysical models. Those errors are typically correlated in time and space, and are distributed all over the globe as a complex function of latitude, orography, and other factors. Since those dependencies are difficult to describe analytically, hydrodynamic model errors are typically approximated from an ensemble of model realizations that are implicitly assumed to be equally probable. We follow this approach by analyzing

pressure anomaly data from a small ensemble of four up-to-date atmospheric and oceanic model data-sets available to us for the year 2006.

It should be noted that errors at temporal scales larger than 30 days that also include, e.g., apparent jumps in the atmospheric pressure due to changes in the orography of the operational ECMWF model (e.g., *Duan et al.*, 2012) will not be considered. Errors at those temporal scales map directly into the monthly gravity fields as systematic biases, but do not contribute to the variability within the month and therefore do not actually lead to de-aliasing errors. Such monthly biases might be corrected a posteriori by means of subtracting an alternative reference model, whereas de-aliasing errors cannot be removed from the monthly-mean gravity fields with post-processing methods (*Forootan et al.*, 2014).

The updated ESM intended to serve as a source model in future mission simulations covers the period 1995 – 2006. Yet, it would be convenient to have a perturbed de-aliasing model available for the same period. Since the original ESM of *Gruber et al.* (2011) covers that time-frame as well, we use differences between those two data-sets as a basis for a series of error realizations. This choice is moreover justified by the fact that the original ESM is partly based on ECMWF's previous re-analysis ERA-40 (*Uppala et al.*, 2005) and an earlier OMCT experiment (*Dobslaw and Thomas*, 2007), which have been both part of the now outdated GRACE AOD1B release 04. Thus, the difference between the two ESMs with its very complex spatial and temporal correlations is representative for errors contained in AOD1B only three years ago.

To account for likely model improvements after the release 04 of AOD1B and/or common errors in the original and the updated ESM, we will subsequently scale those differences with constant coefficients for land and ocean regions in order to match the spread of the ensemble of current state-of-the-art model data-sets for the year 2006 at large spatial scales up to approximately spherical harmonic degree and order (d/o) 60. Since we expect a frequency dependence of the scaling coefficients, we will dissect all model differences from the ensemble and also the two ESMs by a series of 3rd order Butterworth filters into five different bands covering periods of 10 – 30 days, 3 – 10 days, 1 – 3 days, the S1 atmospheric tide, and the sub-diurnal periods. In the following, we describe our procedure for the 10 – 30 days band explicitly. Please note that the ensemble spread related to signals at intermediate spatial scales over the oceans will be covered in particular by the third error component due to omitted physical processes, which will be introduced later in Sect. 4.

One member of the small ensemble of atmospheric model data-sets is the current global re-analysis of the ECMWF, ERA-Interim (*Dee et al.*, 2011) that is also used for the updated ESM. In addition, we use the Climate Forecast System Reanalysis (CFSR; *Saha et al.*, 2010) prepared by the National Center for Environmental Prediction, and NASA's Modern Era Retrospective Analysis for Research and Applications (MERRA; *Rienecker et al.*, 2011). The fourth data source is the operational ECMWF analysis data-set that is also used for AOD1B. In order to assess the current level of uncertainties in global models of atmospheric mass variability over the continents, we calculate pairwise rms differences of atmospheric surface pressure that are bandpass filtered to contain only variability with periods of 10 – 30 days over the year 2006 (Fig. 1). For closely related models, as, e.g., operational and re-analysis data from ECMWF, we note globally fairly homogeneous residuals of about 0.2 hPa only, which is equivalent to a 2 mm change in

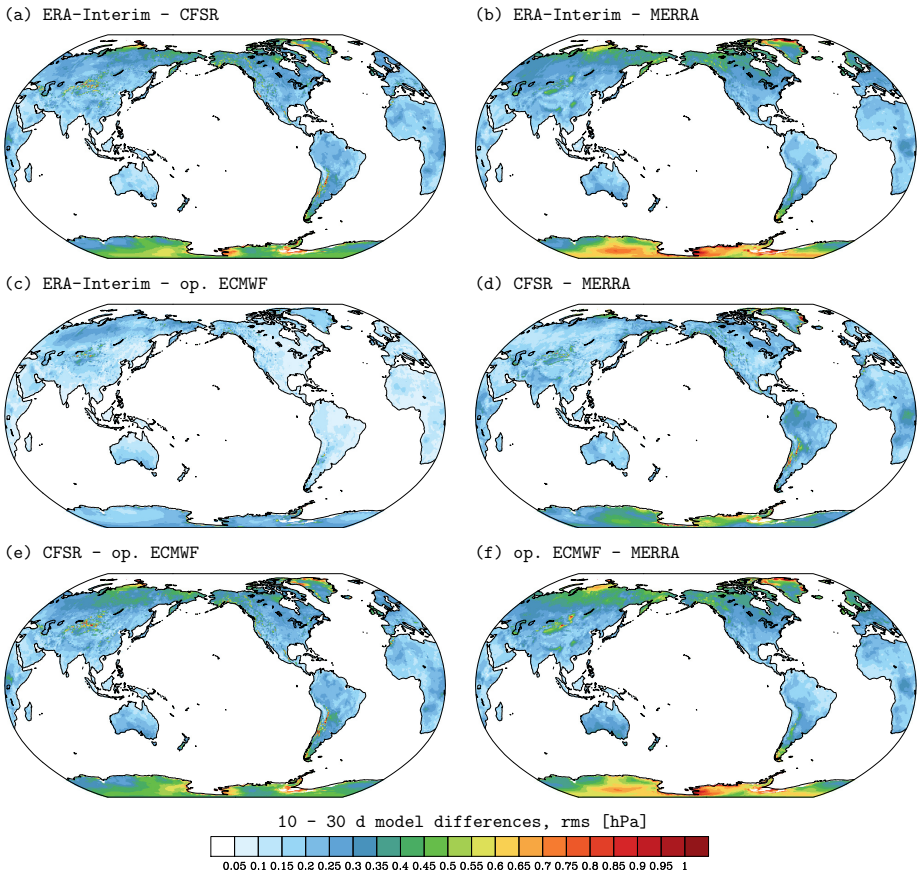

Fig. 1 Rms differences of band-pass filtered atmospheric mass variability from four different global atmospheric surface pressure data-sets at periods of 10 – 30 days for the year 2006: ERA-Interim re-analysis, MERRA re-analysis, CFSR re-analysis, and ECMWF operational analysis

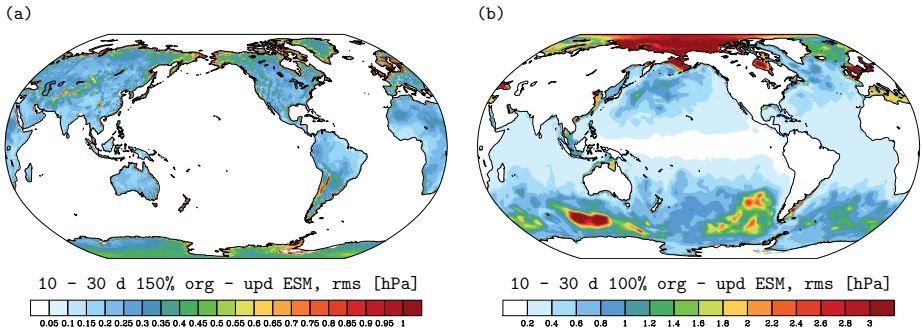

Fig. 2 Rms of re-scaled atmospheric surface pressure (left) and ocean bottom pressure (right) errors with large spatial scales at periods of 10 – 30 days as averaged over the period 1995 – 2006

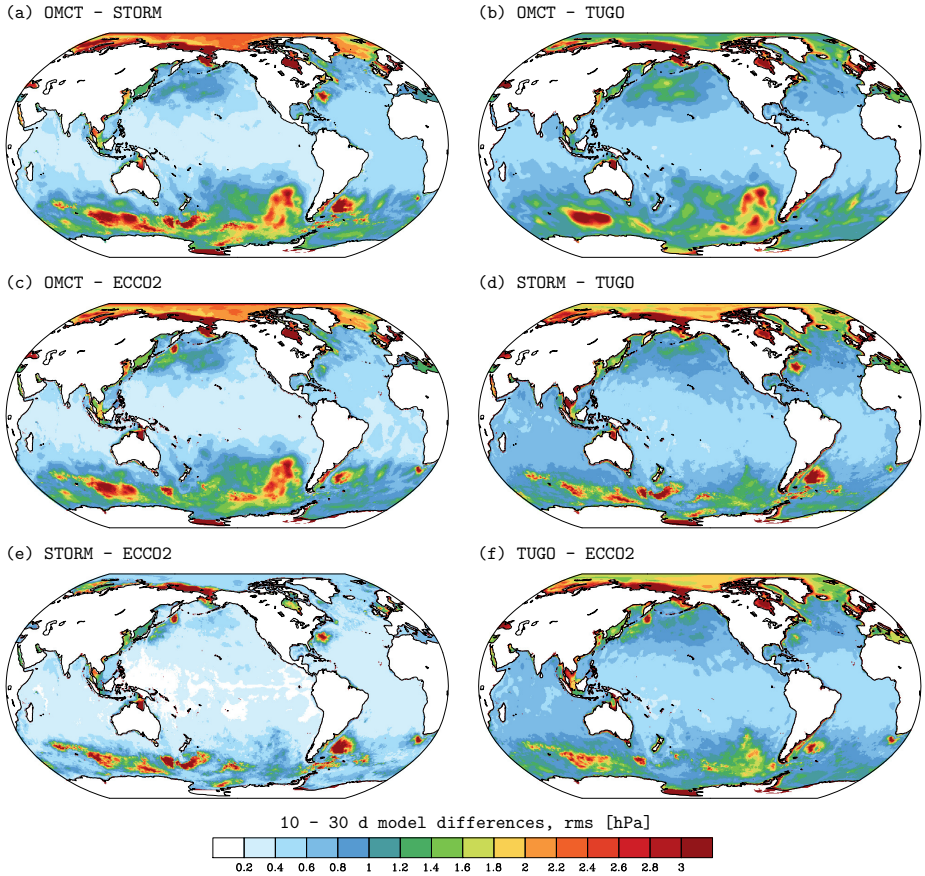

Fig. 3 Rms differences of band-pass filtered ocean bottom pressure variability from four different global ocean models at periods of 10 – 30 days for the year 2006: OMCT as used for AOD1B RL05, TUGO, ECCO2, and MPIOM STORM

water height. The spread is substantially larger when any of the ECMWF models is compared with CFSR or MERRA, culminating in rms differences of up to 0.7 hPa in Antarctica. Based on the pairwise model comparison, we conclude that the spread between the two ESMs underestimates the uncertainty. We therefore up-scale the atmospheric component by 150% for periods of 10 – 30 days (Fig. 2a).

The ensemble of ocean model data-sets consists of a simulation from OMCT forced with ERA-Interim atmospheric data, the STORM experiment performed with the Max-Planck-Institute for Meteorology Ocean Model (MPIOM) that uses NCEP2 atmospheric data (*von Storch et al.*, 2012), and a recent run with the french TUGO model (*le Bars et al.*, 2010) under ERA-Interim forcing that is contained in the alternative AOD coefficients provided by GRGS. Finally, we utilize the ECCO2 ocean synthesis performed at JPL (cube92; *Menemenlis and Campin*, 2008) that assimilates a vast range of different oceanographic observations. We note rather small differences between STORM and ECCO2 that both lack forcing

Table 1 Scaling Coefficients for continental and oceanic regions applied to the model differences of the original and the updated ESM for the realization of de-aliasing errors at large spatial scales for five different frequency bands

	Continents	Oceans
10 – 30 days	150%	100%
3 – 10 days	250%	100%
1 – 3 days	350%	150%
S_1(p)	250%	150%
sub-diurnal	180%	150%

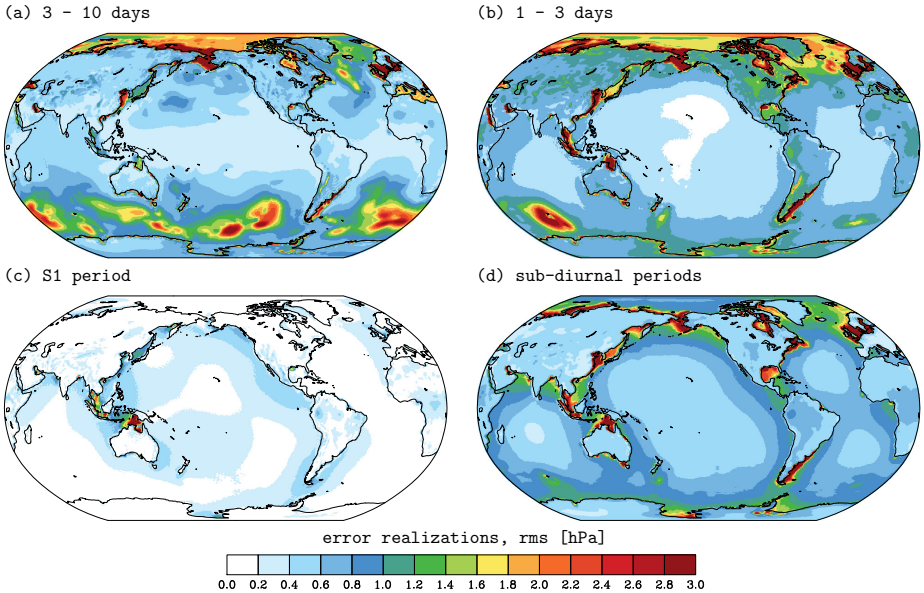

Fig. 4 Rms of the sum of the re-scaled atmospheric surface and ocean bottom pressure errors at large spatial scales with periods of (a) 3 – 10 days, (b) 1 – 3 days, (c) the S1 atmospheric tide, and (d) sub-diurnal periods over the period 1995 – 2006

from atmospheric pressure variability and thereby miss a small but non-negligible part of the energy input from the atmosphere into the oceans (Fig. 3). This is in particular relevant for the Arctic Ocean, where the inverse barometric adjustment to atmospheric pressure changes is hampered by the narrow straits connecting the basin to the Pacific and the North Atlantic. Residuals of all pairwise model differences show a clear zonal structure, where larger errors are found in regions with larger signal variability. Based on those comparisons, we conclude that the uncertainty associated with ocean bottom pressure variability for periods of 10 – 30 days is well represented by the spread between the two ESMs (Fig. 2b).

Similar assessments are performed for the periods of 3 – 10 days, 1 – 3 days, the S1 atmospheric tide, as well as the sub-diurnal periods; details are given in *Bergmann-Wolf et al.* (2015). The estimated scaling coefficients (Tab. 1) indicate that the original and the updated ESM tend to converge for higher frequencies, thereby requiring stronger up-scaling at shorter periods. This is consistent with

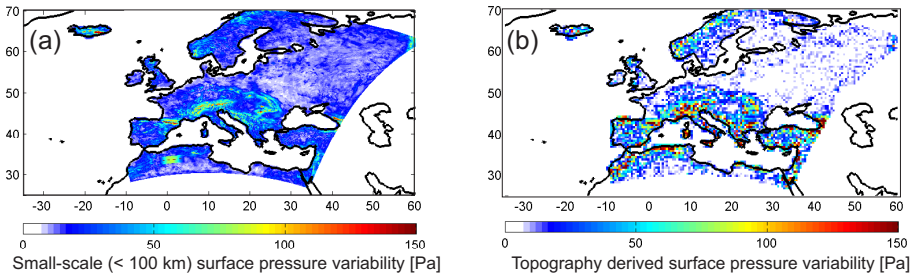

Fig. 5 Rms variability of pressure signals at small spatial scales from the high-resolution regional model COSMO-EU that are typically missed out by global atmospheric re-analysis data-sets (a), and a reconstruction of small-scale atmospheric error variability from a regression model based on the local orographic roughness (b)

our findings from the pairwise model comparison, since similar modelling assumptions and common errors included in two closely related model realisations tend to have an increasing influence at higher frequencies. The spatial variability of errors in the different frequency bands are summarized in Fig. 4. For the continents, error patterns of atmospheric surface pressure are fairly homogeneous over all latitudes at all periods considered. For the oceans instead, we find distinctly latitude-dependent errors at in particular lower frequencies with almost no errors in the tropics and highest values at extra-tropical latitudes (40° – 60° N and S) characterized by strong westerly winds. In addition, we note that a number of sub-surface oceanic basins have distinctly different resonance frequencies that lead to peak error levels in particular sectors of the Southern Ocean for the various periods considered, as, e.g., the Bellingshausen Basin (60° S, 60° W) or the Australian Antarctic Basin (50° S, 100° E). For more rapid processes at diurnal periods and beyond, errors are rather dominated by basin-wide modes, resembling the typical tidal resonances at those frequencies.

3 AOD Errors at Small Spatial Scales

Global atmospheric re-analyses often used for the derivation of AOD coefficients are confined to the representation of atmospheric dynamics, land-atmosphere interactions, and orography at large spatial scales only, since the discretization of the model equations in time and space requires the parametrization of local processes from a certain threshold on. Both ESM data-sets are expanded in Stokes coefficients up to d/o = 180, which roughly corresponds to a spatial resolution of 1°, but there is certainly variability at spatial scales below that threshold in both atmosphere and oceans.

To assess signals at small spatial scales not covered explicitly by the updated ESM, we utilize data from a recent experiment with the non-hydrostatic high-resolution numerical weather prediction model COSMO-EU (*Baldauf et al.*, 2011). The model is discretized over Europe with a horizontal resolution of approximately 7 km. Available to us is an operational analysis run for the year 2006 with daily sampling. To isolate small-scale variability at high frequencies, a high-pass filter with 30 days cutoff period is applied to the surface pressure anomalies. Sub-

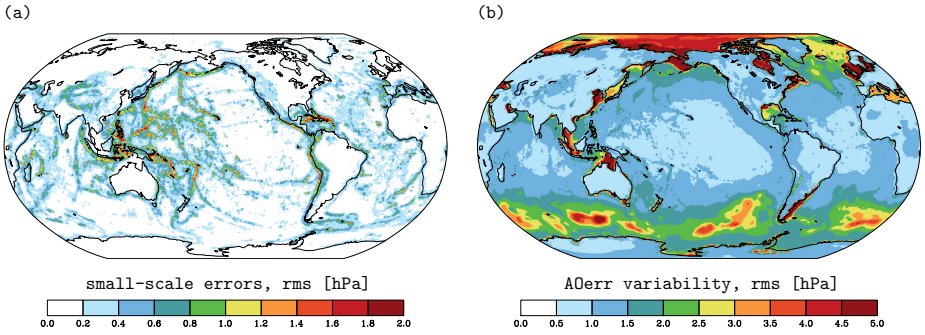

Fig. 6 Rms errors at small spatial scales obtained from a regression model based on COSMO-EU (a), and rms variability of the component AOerr of the realistically perturbed de-aliasing model that summarizes errors at both large and small spatial scales (b)

sequently, 1° spatial averages are removed from the high-pass filtered pressure anomalies to retain only signals at spatial scales smaller than approximately 100 km. Rms values of those residuals are as large as 1.5 hPa in mountaineous regions as, e.g., the Alps and the Pyrenees (Fig. 5a). Those signals are highly localized and in particular confined to areas with very rough orography. Most other regions instead, show residual pressure signals that are well below 0.5 hPa.

Since high-resolution model data is only available to us from an atmospheric model over a limited domain, we extrapolate small-scale errors to the whole globe by hypothesizing a linear relationship between the roughness of the orography and residual pressure signals at small spatial scales (see also, e.g., *van Dam et al.*, 2010). To obtain a roughness scale, we smooth the global orography data-set ETOPO2 that also includes sub-surface ocean bathymetry at its original spatial resolution of 2′ by a two-dimensional moving average filter with a window lenghth of 30 grid cells. The difference between the original topography and the smoothed version is taken as an orographic roughness indicator for the regression model. Small-scale pressure variability as obtained from orographic roughness and the regression model at a 0.5° spatial resolution approximates the signal quite well over land (Fig. 5b). We now randomly sample normal distributions with the error variances at small spatial scales derived from the regression model to arrive at a series of 250 independent daily realizations that are subsequently cycled for about 18 times to cover the full 12 year-long period of the updated ESM (Fig. 6a). Regions covered by high mountains as the Himalaya or the Andes dominate the small-scale errors on the continents, whereas deep-sea trenches and sub-ocean ridges are clearly discernable in the oceanic regions. Errors are spatially highly variable and approach 2 hPa in isolated places only.

In order to validate our extrapolation approach, we show rms variability of pressure signals at small spatial scales from two moderate resolution global models – the operational analyses of ECMWF and the MPIOM STORM experiment (*von Storch et al.*, 2012) for January 2011 and 2006, respectively – that have been obtained by applying a Gaussian high-pass filter with 100 km half-wavelength to the daily pressure anomaly grids (Fig. 7). Both data-sets have an approximate spatial resolution of 0.1° which is more than twice the sampling of COSMO-EU. We note very good correspondence with the orography-based error predictions over the

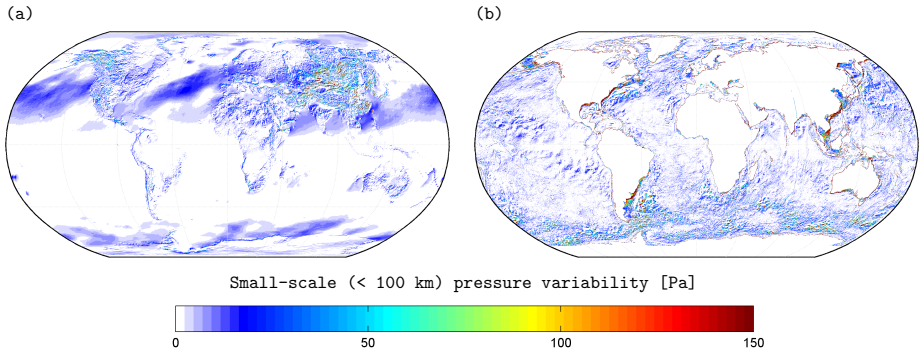

Fig. 7 Rms variability of pressure signals at small spatial scales from the global ECMWF numerical weather prediction model (a), and the global ocean model experiment STORM performed with the MPIOM ocean model (b), both obtained by high-pass filtering the original daily pressure anomalies at 0.1° with a Gaussian smoother of 100 km half-wavelength from 30 days of data during January 2011 and 2006, respectively

continents that fully justifies our approach in those regions. For the oceans, however, pattern deviate substantially: small-scale signals in the STORM experiment are rather concentrated along the coasts and do show only moderately enhanced amplitudes at bathymetric structures as deep-sea trenches. Since nevertheless the signal amplitudes approaching 150 Pa in isolated places only are consistent with our extrapolation approach, we conclude that the small-scale errors predicted over the oceans are indeed suitable to initially test the relevance of such small-scale features for satellite gravimetry. For a more rigorous assessment of the impact of small-scale errors on future satellite gravity mission concepts, as, e.g., a satellite-mounted quantum gradiometer, a revision of this error model component based on high-resolution global atmosphere and ocean model experiments should be attempted.

4 Oceanic Signals Omitted in AOD Models

The oceanic components of all currently available AOD models rely on either barotropic (*Carrère and Lyard*, 2003) or baroclinic (*Thomas et al.*, 2001) global ocean circulation models forced with atmospheric data from numerical weather models that do not assimilate any type of high-frequency observational data. Such simulations typically exclude meso-scale variability and small-scale eddies, which are primarily near-surface features but partially have also bottom pressure signatures in particularly energy-rich areas of the world's ocean (*Kuhlmann et al.*, 2013). In addition, those models typically do not include changes in global barystatic sea-level (*Chambers*, 2004), which causes a seasonal variation of the globally averaged ocean bottom pressure of about 1 hPa.

To account for those principal deficits of presently available AOD products in future mission studies, we derive a set of unperturbed AOD coefficients for the updated ESM. In continental regions it is identical to the atmospheric part of the updated ESM, but the oceanic component is only based on the OMCT model run and excludes the small-scale variability from MPIOM STORM (*von Storch*

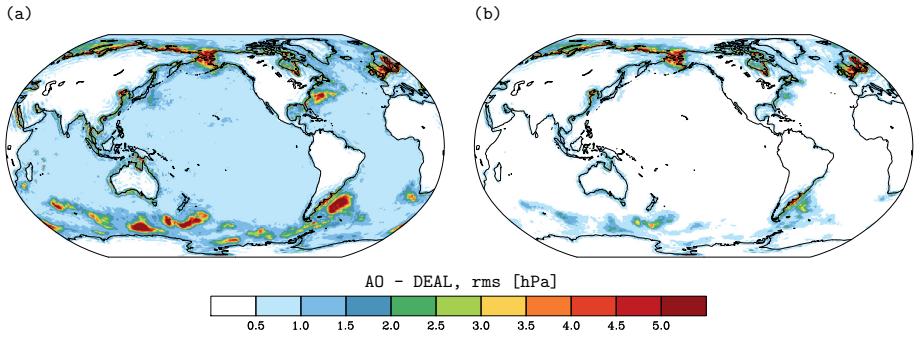

Fig. 8 Rms differences (a) and rms of 30 days high-pass filtered differences (b) between the atmospheric and oceanic (AO) component of the updated ESM and the DEAL component of the realistically perturbed de-aliasing model calculated over the period 1995 - 2006, which reflect the impact of physical processes in the ocean that are currently not represented in release 05 of AOD1B

et al., 2012) and the barystatic sea-level variability that have been added into the updated ESM. Rms differences therefore deviate from zero only over the oceans (Fig. 8a), where a globally homogeneous signal of about 0.7 hPa rms related to seasonal changes in total ocean mass dominates. In addition, we find areas with distinctly large residuals of more than 5 hPa in oceanic regions characterized by high eddy kinetic energy, and small-scale mass variability all along the coasts. Signal magnitudes drop substantially, however, when only high-pass filtered variability at periods shorter than 30 days is considered (Fig. 8b), which is the part of the signal that actually contributes to the de-aliasing errors. High-pass filtered signals in the open ocean are well below 1 hPa, thereby indicating that global ocean simulations that are not eddy-resolving are sufficiently well suited to serve as de-aliasing model for high-frequency bottom pressure variability.

5 Two New Components of the Updated Earth System Model: AOerr and DEAL

To allow for a straightforward implementation of those AOD-related errors in future satellite mission simulation studies, two series of Stokes coefficients up to d/o = 180 with a time sampling of 6 hours over the full 12-year time-period of the updated ESM are made publicly available via doi:10.5880/GFZ.1.3.2014.001. First, the "DEAL" coefficients contain the unperturbed de-aliasing model introduced in the previous section. It might be used as a background model for satellite simulation studies in case that – apart from the principal deficits indicated above – perfect model-based predictions of atmospheric and oceanic mass variability should be assumed. If even the removal of those principal model deficits appears plausible until the anticipated launch date of a future mission, a replacement of DEAL with the sum of the amospheric and oceanic components of the updated ESM might be considered.

Secondly, the "AOerr" coefficients consist of the sum of the error series at small spatial scales as well as at large spatial scales at all five frequency bands

discussed above. AOerr needs to be added to DEAL to arrive at a reasonably perturbed AOD model. Time series of AOerr at individual geographic positions have zero mean over the 12-year period of data provided and an approximately stationary variance when individual years are considered (*Bergmann-Wolf et al.*, 2015). The overall variability of AOerr (Fig. 6b) is dominated by large-scale errors over the oceans with particularly high error magnitudes in the Arctic Ocean and in the vicinity of the Antarctic Circumpolar Current. Continental regions show a comparatively homogeneous error level, although slightly higher rms values are found in glaciated regions at polar latitudes. Errors at small spatial scales instead tend to have a minor influence only. For satellite simulation experiments aiming at satellite scenarios in a rather distant future, a reduction of those AOerr coefficients by means of a global factor might be performed in order to account for anticipated future improvements in the accuracy of those models until launch.

6 Variance Component Estimation from GRACE

In the following, we are going to contrast the newly derived series of error realizations against GRACE-based estimates of high-frequency mass variability. The recently published ITSG-Grace2014 release (*Mayer-Gürr et al.*, 2014) contains in addition to long-term and monthly-mean global gravity fields also a series of daily solutions based on a Kalman Smoother approach (*Kurtenbach et al.*, 2009, 2012). The large-scale signals at periods down to a few days contained in the predecessor of this daily series have been found to be geophysically plausible both on the continents (*Zenner et al.*, 2014) and over the oceans (*Bergmann and Dobslaw*, 2012) from comparisons with independent in situ observations and numerical model estimates. From the daily normal equations of ITSG-Grace2014 expanded into spherical harmonics up to d/o = 40 we remove all signals at periods longer than 30 days by estimating and subtracting the long-term mean and drift as well as subsequently also the monthly-mean components. Since all standard time-variable background models for solid Earth tides, ocean tides, and also non-tidal variability from AOD1B release 05 have been applied, we expect that the remaining residuals only contain GRACE system noise, sub-monthly variations in terrestrially stored water, episodic seismic events, and errors in background models applied.

To separate different contributors to the GRACE residuals we describe their stochastic behaviour by a number of variance-covariance matrices, implicitly assuming that each of the components is stationary in time. Those covariance matrices for the remaining atmospheric and oceanic signals are calculated from the 12 year-long series of non-tidal atmosphere and ocean error realizations. We dissect the AOerr series into nine different regions of the world: the Arctic Ocean, the oceans at the Northern Hemisphere between 23°N – 67°N, the tropical oceans, and the southern oceans at latitudes below 23°S. Continental areas are divided into Antarctica, Greenland, the northern hemispheric continents at latitudes above 23°N except for Greenland, the tropical continents, and the southern hemispheric continents at 23°S – 60°S. To additionally account for sub-monthly water storage changes on the continents that might be eventually correlated to atmospheric errors, we also derive empirical covariances out of the continental components of the updated ESM containing ice mass and terrestrial water storage changes that are

Table 2 Area-weighted average rms at large spatial scales up to d/o = 40 and for periods of 1 – 30 days in nine different regions of the globe as contained in the updated ESM (a priori) and derived from two variance component estimation experiments with consistently pre-processed daily normal equations from ITSG-GRACE2014 (a posteriori)

		ESM a priori [hPa]	ITSG-GRACE2014 a posteriori [hPa]	
			individual	summarized
Antarctica	surface pressure	0.81	1.16	-
	ice mass change	0.13	0.52	-
	sum	0.82	-	1.26
Greenland	surface pressure	0.66	1.27	-
	ice mass change	0.21	0.50	-
	sum	0.69	-	1.36
northern continents	surface pressure	0.61	1.15	-
(23°N – 80°N)	terrestrial water	0.35	0.64	-
	sum	0.70	-	1.26
southern continents	surface pressure	0.58	1.06	-
(23°S – 60°S)	terrestrial water	0.48	0.68	-
	sum	0.75	-	1.23
tropical continents	surface pressure	0.50	0.63	-
(23°S – 23°N)	terrestrial water	0.43	1.04	-
	sum	0.66	-	1.27
tropical oceans	bottom pressure	0.65	0.76	0.76
Arctic Ocean	bottom pressure	2.83	3.01	3.03
northern oceans	bottom pressure	1.41	1.21	1.21
southern oceans	bottom pressure	1.68	1.27	1.28

filtered for periods of 1 – 30 days as well, leading to in total 14 covariance matrices solely for the non-tidal geophysical signals.

The sum of all covariance matrices is expected to describe the stochastic characteristics of the daily GRACE solutions. The method of variance component estimation (VCE; *Koch and Kusche*, 2002) allows for estimating pre-factors for each covariance matrix in an iterative procedure. Those variance factors obtained from the VCE are subsequently multiplied by the prior variances and transformed into area-weighted rms (wrms) values. By comparing prior wrms estimates from the updated ESM with a posteriori results from the VCE (Tab. 2), we note that the level of errors derived in this study is generally confirmed by ITSG-Grace2014. For the continents, GRACE-based wrms are typically 0.4 hPa larger than predicted by AOerr, which is very well acceptable since additional non-atmospheric error contributors to the GRACE normal equations at this level cannot be entirely excluded. A second VCE experiment utilizing only 9 instead of 14 empirical error covariance matrices by summing atmospheric errors and short-term water storage changes beforehand (Tab. 2; third column) indicates weak correlations between atmospheric mass variability errors and sub-monthly water storage changes, but generally confirms that ITSG-Grace2014 contains slightly higher variability over the continents than predicted by AOerr and the sub-monthly water storage variability contained in the updated ESM. Over the oceans, the substantially higher error levels contained in AOerr are also confirmed by GRACE. The exceptionally strong wrms of about 3 hPa in the Arctic Ocean in particular is seen by GRACE as well, whereas the errors in the extra-tropical oceans at both hemispheres are found

to be modelled slightly too large. We nevertheless note that differences between the prior estimates and the GRACE-based results never exceed 0.5 hPa in wrms both on continents and in the oceans, letting us conclude that the error realization series provided in AOerr realistically represents the current level of AOD1B accuracy for spatial scales up to d/o = 40 and periods of 1 – 30 days.

7 Simulated Aliasing Errors for Future Missions

We finally attempt to estimate the spatial characteristics of temporal aliasing errors for a set of different GRACE-type satellite constellations to provide evidence for the relative importance of such type of errors for a small range of plausible future mission scenarios. We use the simulation setting described by *Flechtner et al.* (2015), who recently performed an in-depth assessment of the upcoming GRACE-FO mission and its expected contributions to Earth science applications. We perform four twin experiments ranging each over the three months April – June 2005 that all assume satellites in pearl-string formation connected by microwave intersatellite links at altitudes of 480 km. The scenarios include (i) a single polar mission, (ii) a single polar mission with an orbital plane shifted by 90° in right ascension, (iii) a combination of two polar pairs separated by 90° in right ascension, as well as (iv) one polar pair and a second pair in an 70° inclined orbit, which is typically referred to as a Bender-type constellation.

For any twin experiment, two monthly global gravity fields are retrieved up to d/o = 100 that differ only in the applied a priori background model: by applying the atmospheric and oceanic (AO) component of the updated ESM, we perfectly remove all atmosphere and ocean mass variability signals, whereas the use of the realistically perturbed de-aliasing model AOerr+DEAL is expected to cause residual variability. Differences between the two retrievals are interpreted as de-aliasing errors. Note that further processes leading to temporal aliasing – as, e.g., ocean tides and sub-monthly water storage variations – included in *Flechtner et al.* (2015) are treated identically in both retrievals and are therefore not visible in the results discussed below.

Differences between finally retrieved gravity fields for May 2005 reveal the spatial characteristics of the de-aliasing errors introduced by imperfect time-variable background models (Fig. 9). For the unfiltered geoid heights of both single-pair polar mission experiments, we note substantial de-aliasing errors at moderate latitudes – where much of the signal variability in atmosphere and oceans resides and thus the errors are larger – and also at tropical latitudes, where the spatial sampling of a polar-orbiting mission is poor. For a combination of two polar pairs, we see a moderate reduction of de-aliasing errors on the finally retrieved gravity field by 14% that are distributed quite homogeneously over all latitudes. For the Bender-type constellation, we find a substantial reduction by more than 69%, indicating that the rotated error anisotropy due to the modified azimuth of the inter-satellite link of an inclined pair stabilizes the monthly gravity field solution substantially. Nevertheless, for the Bender-type constellation, the reduction of aliasing artifacts is not homogeneous over the globe: de-aliasing errors in regions not sampled by the second pair are as high as for a single pair mission in a polar orbit.

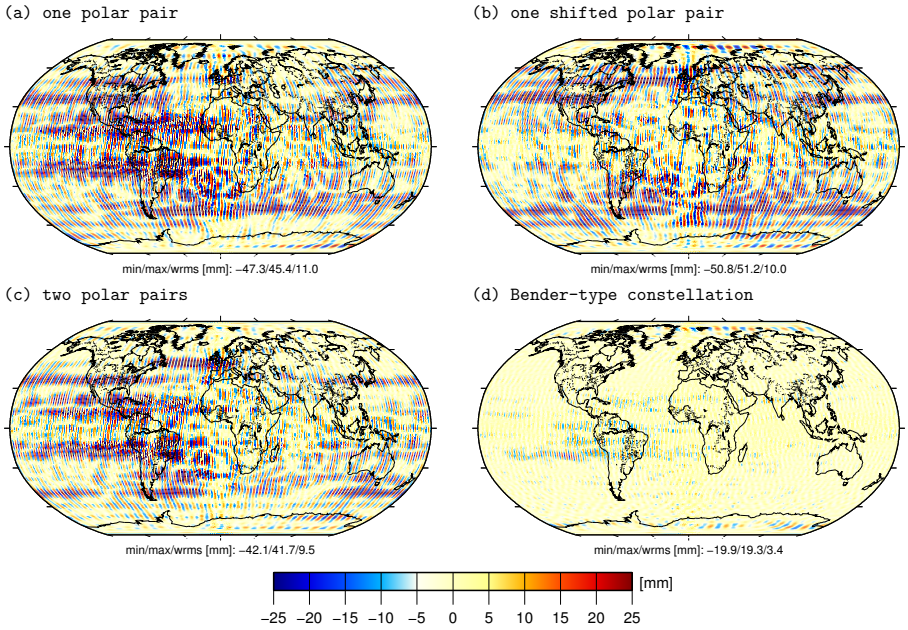

Fig. 9 Geoid height errors introduced into simulated gravity field retrievals from imperfect background models of non-tidal atmosphere and ocean variability for May 2005: (a) polar pair, (b) polar pair shifted by 90° in right ascension, (c) two polar pairs, and (d) a polar pair and a 70° inclined pair

Similar levels of reduction are obtained for April and June 2005 with 38% and 34%, respectively, for two polar pairs, and 62% and 77% for the Bender-type constellation (not shown). In terms of degree amplitudes (Fig. 10), we note that AOD1B errors start dominating the solutions at around d/o = 30 on a global average. For two polar pairs, improvements are visible starting at d/o = 15, and AOD1B errors only dominate from d/o = 40 onwards. Best results are expected from a Bender-type constellation with a second pair in a moderately inclined orbit, that extends this threshold even further to d/o = 45 and reduces the impact of AOD1B errors on the monthly solutions even on higher degrees and orders by a substantial amount.

8 Summary

A realistically perturbed synthetic de-aliasing model consistent with the updated Earth System Model is now available over the period 1995 – 2006. The model contains (i) errors at large spatial scales that were assessed individually for five different frequency bands, (ii) errors at small spatial scales typically not treated by global atmospheric and oceanic models, and (iii) errors due to mass variability in the oceans that is currently not included in any of the available AOD products. The realistically perturbed de-aliasing model is publicly available in two sets of spherical harmonic coefficients: the AOerr coefficients represent a summarized re-

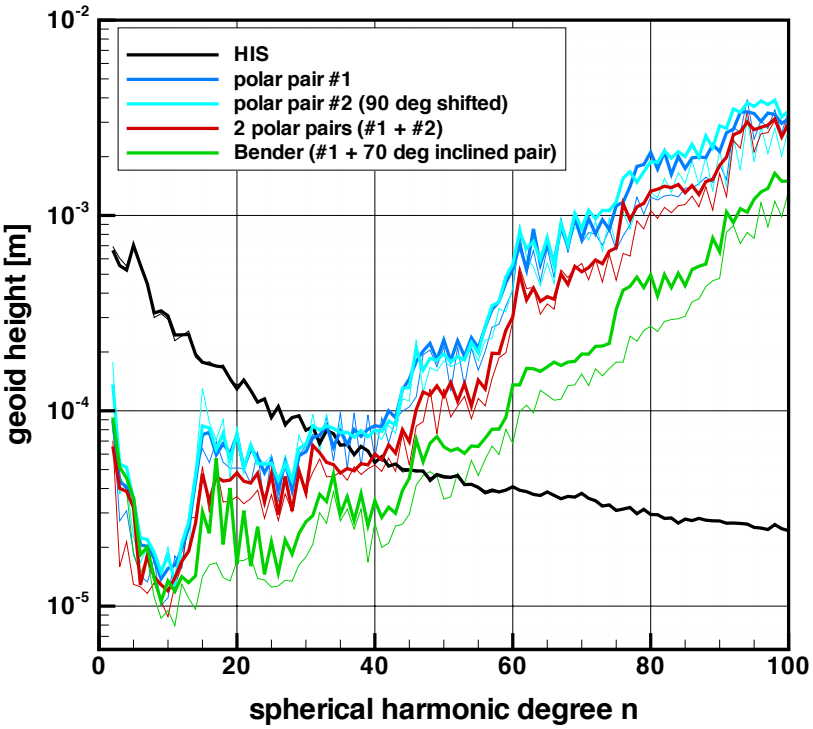

Fig. 10 Geoid height error degree amplitudes introduced into the simulated gravity field retrievals from imperfect background models of non-tidal atmosphere and ocean variability for May 2005 (thin lines) and averaged over three simulated months covering April – June 2005 (thick lines)

alisation of errors at large and small spatial scales, whereas the DEAL coefficients differ from the AO component of the updated ESM only by absent bottom pressure anomalies related to barystatic sea-level changes and meso-scale dynamics. By providing those two separate components, we offer users some flexibility to account for potential improvements in AOD model quality until the anticipated launch date of mission – be it by a reduction of the overall noise level or by the additional inclusion of further ocean processes into AOD products.

Magnitudes of the errors contained in the perturbed de-aliasing model were derived from analyzing a small ensemble of four atmospheric and oceanic data-sets. For large spatial scales up to d/o = 40 and periods longer than 24 h, those error levels were generally confirmed from a variance component estimation based on ITSG-Grace2014 daily normal equations. The perturbed error model is thus believed to be representative for the present-day errors contained in AOD1B RL05. Initial full-scale future satellite mission performance simulations with this perturbed de-aliasing model indicated that for GRACE-like satellites only moderate reductions of de-aliasing errors can be expected from two satellite pairs in polar

orbits. Substantially larger improvements were found for a so-called Bender constellation, where a polar pair is augmented by a second pair of satellites in an moderately inclined orbit, which greatly stabilizes the gravity field solution due to its rotated sampling sensitivity. Since both the source model and the perturbed de-aliasing model are publicly available, similar experiments might be now performed with alternative gravity mission simulation tools in order to increase the robustness of conclusions derived from such assessments.

Acknowledgements This study was performed under contract No. 4000109421 with the European Space Agency (ESA). We thank Deutscher Wetterdienst, Offenbach, Germany, and the European Centre for Medium-Range Weather Forecasts for providing data from ECMWF's latest reanalysis ERA-Interim. Numerical simulations were performed at Deutsches Klimarechenzentrum, Hamburg, Germany. The updated Earth System Model and the corresponding realistically perturbed AOD model as described in this paper are publicly available at doi:10.5880/GFZ.1.3.2014.001.

References

Baldauf, M., A. Seifert, J. Förstner, D. Majewski, M. Raschendorfer, and T. Reinhardt (2011), Operational Convective-Scale Numerical Weather Prediction with the COSMO Model: Description and Sensitivities, *Mon. Weather Rev.*, *139*, 3887–3905, doi:10.1175/MWR-D-10-05013.1.

Bergmann, I., and H. Dobslaw (2012), Short-term transport variability of the Antarctic Circumpolar Current from satellite gravity observations, *J. Geophys. Res.*, *117*(C5), 1–12, doi:10.1029/2012JC007872.

Bergmann-Wolf, I., E. Forootan, V. Klemann, J. Kusche, and H. Dobslaw (2015), Updating ESA's Earth System Model for Gravity Mission Simulation Studies: 3. A Realistically Perturbed Non-Tidal Atmosphere and Ocean De-Aliasing Model, *Tech. rep.*, Scientific Technical Report 14/09, GFZ, doi:10.2312/GFZ.b103-14091.

Boy, J.-P. (2005), Precise evaluation of atmospheric loading effects on Earth's time-variable gravity field, *J. Geophys. Res.*, *110*(B8), 1–10, doi:10.1029/2002JB002333.

Carrère, L., and F. Lyard (2003), Modeling the barotropic response of the global ocean to atmospheric wind and pressure forcing - comparisons with observations, *Geophys. Res. Lett.*, *30*(6), 1997–2000, doi:10.1029/2002GL016473.

Chambers, D. P. (2004), Preliminary observations of global ocean mass variations with GRACE, *Geophys. Res. Lett.*, *31*(13), 1–4, doi:10.1029/2004GL020461.

Dee, D. P., et al. (2011), The ERA-Interim reanalysis: configuration and performance of the data assimilation system, *Q. J. Roy. Met. Soc.*, *137*(656), 553–597, doi:10.1002/qj.828.

Dobslaw, H., and M. Thomas (2007), Simulation and observation of global ocean mass anomalies, *J. Geophys. Res.*, *112*(C5), C05,040, doi:10.1029/2006JC004035.

Dobslaw, H., F. Flechtner, I. Bergmann-Wolf, C. Dahle, R. Dill, S. Esselborn, I. Sasgen, and M. Thomas (2013), Simulating high-frequency atmosphere-ocean mass variability for dealiasing of satellite gravity observations: AOD1B RL05, *J. Geophys. Res.*, *118*(7), 3704–3711, doi:10.1002/jgrc.20271.

Dobslaw, H., I. Bergmann-Wolf, R. Dill, E. Forootan, V. Klemann, J. Kusche, and I. Sasgen (2015), The updated ESA Earth System Model for future gravity mission simulation studies, *J. Geod.*, doi:10.1007/s00190-014-0787-8.

Duan, J., C. K. Shum, J. Guo, and Z. Huang (2012), Uncovered spurious jumps in the GRACE atmospheric de-aliasing data: potential contamination of GRACE observed mass change, *Geophys. J. Int.*, *2*, 1–5, doi:10.1111/j.1365-246X.2012.05640.x.

Elsaka, B., J.-C. Raimondo, P. Brieden, T. Reubelt, J. Kusche, F. Flechtner, S. Iran Pour, N. Sneeuw, and J. Müller (2014), Comparing seven candidate mission configurations for temporal gravity field retrieval through full-scale numerical simulation, *J. Geod.*, *88*(1), 31–43, doi:10.1007/s00190-013-0665-9.

Famiglietti, J. S., and M. Rodell (2013), Water in the balance, *Science (80-.).*, *340*(61), 1300–1301, doi:10.1126/science.1236460.

Flechtner, F., and H. Dobslaw (2013), GRACE AOD1B Product Description Document for Product Release 05, *Tech. rep.*, Rev. 4.0, GRACE Document 327-750, GeoForschungsZentrum Potsdam.

Flechtner, F., P. Morton, M. Watkins, and F. Webb (2014), Status of the GRACE Follow-On Mission, in *IAG Symp. Gravity, Geoid, Height Syst. Int. Assoc. Geod. Symp. 141*, edited by U. Marti, Springer, doi:10.0007/978-3-319-10837-7-15.

Flechtner, F., K.-H. Neumayer, C. Dahle, H. Dobslaw, A. Güntner, J.-C. Raimondo, and E. Fagiolini (2015), What can be expected from the GRACE-FO Laser Ranging Interferometer for Earth Science Applications?, *Surv. Geophys.*, doi:10.1007/s10712-015-9338-y.

Forootan, E., O. Didova, J. Kusche, and A. Löcher (2013), Comparisons of atmospheric data and reduction methods for the analysis of satellite gravimetry observations, *J. Geophys. Res.*, *118*(1), 2382–2396, doi:10.1002/jgrb.50160.

Forootan, E., O. Didova, M. Schumacher, J. Kusche, and B. Elsaka (2014), Comparisons of atmospheric mass variations derived from ECMWF reanalysis and operational fields, over 2003-2011, *J. Geod.*, *88*, 503–514, doi:10.1007/s00190-014-0696-x.

Gruber, T., et al. (2011), Simulation of the time-variable gravity field by means of coupled geophysical models, *Earth Syst. Sci. Data*, *3*(1), 19–35, doi:10.5194/essd-3-19-2011.

Gruber, T., et al. (2014), *Earth System Mass Transport Mission (Square) ? Concept for a Next Generation Gravity Field Mission*, 318, 210 pp., Deutsche Geodätische Komission, Series B, Bayerische Akademie der Wissenschaften, Munich.

Han, S.-C., C. Jekeli, and C. K. Shum (2004), Time-variable aliasing effects of ocean tides, atmosphere, and continental water mass on monthly mean GRACE gravity field, *J. Geophys. Res.*, *109*(4), B04,403, doi:10.1029/2003JB002501.

Kim, J. (2000), Simulation study of a low-low satellite-to-satellite tracking mission, Ph.d. thesis, University of Texas, Austin.

Koch, K. R., and J. Kusche (2002), Regularization of geopotential determination from satellite data by variance components, *J. Geod.*, *76*(5), 259–268, doi:10.1007/s00190-002-0245-x.

Kuhlmann, J., H. Dobslaw, C. Petrick, and M. Thomas (2013), Ocean bottom pressure signals around Southern Africa from in situ measurements, satellite data, and modeling, *J. Geophys. Res.*, *118*(10), 4889–4898, doi:10.1002/jgrc.20372.

Kurtenbach, E., T. Mayer-Gürr, and A. Eicker (2009), Deriving daily snapshots of the Earth's gravity field from GRACE L1B data using Kalman filtering, *Geophys. Res. Lett.*, *36*, L17,102, doi:10.1029/2009GL039564.

Kurtenbach, E., A. Eicker, T. Mayer-Gürr, M. Holschneider, M. Hayn, M. Fuhrmann, and J. Kusche (2012), Improved daily GRACE gravity field solutions using a Kalman smoother, *J. Geod.*, *59-60*, 39–48, doi:10.1016/j.jog.2012.02.006.

le Bars, Y., F. Lyard, C. Jeandel, and L. Dardengo (2010), The AMANDES tidal model for the Amazon estuary and shelf, *Ocean Model.*, *31*(3-4), 132–149, doi:10.1016/j.ocemod.2009.11.001.

Loomis, B. D., R. S. Nerem, and S. B. Luthcke (2011), Simulation study of a follow-on gravity mission to GRACE, *J. Geod.*, *86*(5), 319–335, doi:10.1007/s00190-011-0521-8.

Mayer-Gürr, T., N. Zehentner, B. Klinger, and A. Kvas (2014), ITSG-Grace2014: A new GRACE gravity field release computed in Graz, in *Proc. GRACE Sci. Team Meet.*, Potsdam.

Menemenlis, D., and J.-M. Campin (2008), ECCO2: High resolution global ocean and sea ice data synthesis, *Mercat. Ocean Newsl.*, *1*(10), 13–21.

Panet, I., et al. (2012), Earth System Mass Transport Mission (e.motion): A Concept for Future Earth Gravity Field Measurements from Space, *Surv. Geophys.*, *34*(2), 141–163, doi:10.1007/s10712-012-9209-8.

Rienecker, M. M., et al. (2011), MERRA: NASA's modern-era retrospective analysis for research and applications, *J. Clim.*, *24*, 3624–3648, doi:10.1175/JCLI-D-11-00015.1.

Saha, S., et al. (2010), The NCEP climate forecast system reanalysis, *Bull. Am. Meteorol. Soc.*, *91*(August), 1015–1057, doi:10.1175/2010BAMS3001.1.

Sakumura, C., S. Bettadpur, and S. Bruinsma (2014), Ensemble prediction and intercomparison analysis of GRACE time-variable gravity field models, *Geophys. Res. Lett.*, pp. 1389–1397, doi:10.1002/2013GL058632.1.

Sasgen, I., H. Konrad, E. R. Ivins, M. R. Van Den Broeke, J. L. Bamber, Z. Martinec, and V. Klemann (2013), Antarctic ice-mass balance 2003 to 2012: Regional reanalysis of GRACE satellite gravimetry measurements with improved estimate of glacial-isostatic adjustment based on GPS uplift rates, *Cryosphere*, *7*, 1499–1512, doi:10.5194/tc-7-1499-2013.

Tapley, B. D., S. Bettadpur, M. Watkins, and C. Reigber (2004), The gravity recovery and climate experiment: Mission overview and early results, *Geophys. Res. Lett.*, *31*(22), 09,607, doi:10.1029/2004GL019920.

Thomas, M., J. Sündermann, and E. Maier-Reimer (2001), Consideration of ocean tides in an OGCM and impacts on subseasonal to decadal polar motion, *Geophys. Res. Lett.*, *28*(12), 2457–2460.

Thompson, P. F. (2004), Impact of short period, non-tidal, temporal mass variability on GRACE gravity estimates, *Geophys. Res. Lett.*, *31*(6), doi:10.1029/2003GL019285.

Uppala, S. M., et al. (2005), The ERA-40 re-analysis, *Q. J. Roy. Met. Soc.*, *131*(612), 2961–3012, doi:10.1256/qj.04.176.

van Dam, T., Z. Altamimi, X. Collilieux, and J. Ray (2010), Topographically induced height errors in predicted atmospheric loading effects, *J. Geophys. Res.*, *115*(B7), B07,415, doi:10.1029/2009JB006810.

592 Visser, P. N. A. M. (2010), Designing Earth Gravity Field Missions for the Future:
593 A Case Study, in *IAG Comm. 2 GRAVITY, GEOID EARTH Obs. Chania*, pp.
594 131–138.
595 von Storch, J.-S., C. Eden, I. Fast, H. Haak, D. Hernández-Deckers, E. Maier-
596 Reimer, J. Marotzke, and D. Stammer (2012), An Estimate of the Lorenz Energy
597 Cycle for the World Ocean Based on the STORM/NCEP Simulation, *J. Phys.*
598 *Ocean.*, *42*(12), 2185–2205, doi:10.1175/JPO-D-12-079.1.
599 Wiese, D. N., W. M. Folkner, and R. S. Nerem (2009), Alternative mission ar-
600 chitectures for a gravity recovery satellite mission, *J. Geod.*, *83*, 569–581, doi:
601 10.1007/s00190-008-0274-1.
602 Wiese, D. N., R. S. Nerem, and F. G. Lemoine (2012), Design considerations for a
603 dedicated gravity recovery satellite mission consisting of two pairs of satellites,
604 *J. Geod.*, *86*, 81–98, doi:10.1007/s00190-011-0493-8.
605 Zenner, L., T. Gruber, A. Jäggi, and G. Beutler (2010), Propagation of atmospheric
606 model errors to gravity potential harmonics-impact on GRACE de-aliasing, *Geo-*
607 *phys. J. Int.*, *182*(2), 797–807, doi:10.1111/j.1365-246X.2010.04669.x.
608 Zenner, L., I. Bergmann-Wolf, H. Dobslaw, T. Gruber, A. Güntner, M. Watten-
609 bach, S. Esselborn, and R. Dill (2014), Comparison of Daily GRACE Gravity
610 Field and Numerical Water Storage Models for De-aliasing of Satellite Gravime-
611 try Observations, *Surv. Geophys.*, doi:10.1007/s10712-014-9295-x.